The Role of the Interphase on the Shear Induced Failure of Multiwall Carbon Nanotubes Reinforced Epoxy Nanocomposites

Leonel Matías Chiacchiarelli,[1] Mariano Martín Escobar,[1] José María Kenny,[2] Luigi Torre,[2] Analía Vazquez[1]

[1]Instituto de Tecnología de Polímeros y Nanotecnología, CONICET, Construction Department of the Engineering Faculty, University of Buenos Aires, AA1124 Buenos Aires, Argentina
[2]Civil and Environmental Engineering Department, University of Perugia, 05100 Terni, Italy
Correspondence to: L. M. Chiacchiarelli (E-mail: lmchiacchiarelli@yahoo.com.ar)

ABSTRACT: Multiwall Carbon Nanotubes (MWCNT) with an elevated aspect ratio were chemically functionalized with amines and two types of epoxide groups. Thermogravimetric analysis and Fourier Transform-Infrared Spectroscopy (FTIR) analysis corroborated that the functionalization degree was substantial (up to 30 wt %) and the presence of a covalent bond with the MWCNT. The functionalized MWCNT (f-CNT) were incorporated into an epoxy matrix after its dispersion in the diglycidyl ether of bisphenol A (DGEBA) precursor. To induce a shear failure mode, a short-beam (SB) experimental setup was implemented. The SB shear strength (SBSS) proved that the functionalization had a strong influence on its value. For the case of pristine CNT, a neutral effect was obtained. A strong detrimental effect ($-17.2\% \pm 9.5$) was measured for the amine type f-CNT and a positive effect (up to $10.9\% \pm 8.9$) was measured of the epoxide type f-CNT. Fractographic analysis of each formulation was correlated with SBSS performance, proving that the surface texture of the fractured samples was strongly correlated to its value. Furthermore, dynamic mechanical analysis proved that the damping factor and the crosslink molecular weight were correlated with the SBSS performance. A lower full width at half maximum of the damping factor was associated to an improvement of SBSS. © 2014 Wiley Periodicals, Inc. J. Appl. Polym. Sci. **2015**, *132*, 41364.

INTRODUCTION

While laminated fiber reinforced polymer–matrix composite materials have been used successfully in many industries such as aerospace, automobile, marine, military and others, their interlaminar shear strength (ILSS) is usually a limiting design characteristic. This is because conventional manufacturing technologies do not produce laminates with reinforcements oriented in the thickness direction.[1] Improving ILSS has long been an important objective in the fiber reinforced composites field, and to this end, different approaches have been tried out.[1–3] Among them, many researchers have explored the improvement of the ILSS by using fillers with nanometric dimensions, such as carbon nanotubes (CNTs),[4–6] fumed silica,[7] carbon black,[8] and clays,[9] combined with continuous fiber reinforcements. With respect to CNT, their unique mechanical and transporting properties have attracted much interest to develop polymer-based nanocomposites with outstanding mechanical performance and multifunctional characteristics.[10–12] Its utilization to manufacture polymer composites, also denominated nanocomposites,

has revolutionized several fields like electromagnetic shielding, touch screens and materials with static charge dissipation properties[13]. For the case of interlaminar properties, Rahman et al.[14] reported and improvement of ILSS of approximately 50% after adding 0.3 wt % of CNT functionalized with amino groups into a continuous glass fiber-matrix composite. Gojny and coworkers[15] improved the ILSS performance by 16 % after adding 0.3 wt % of double-walled CNTs into fiber reinforced epoxy composites. Even though substantial research has been done combining continuous fibers and fillers with nanometric dimensions, the shear induced failure modes of the composites prepared only with those fillers has not been studied extensively.

Conversely, the outstanding properties of CNTs do not guarantee mechanically superior products because, as in most other types of nanocomposites, the mechanical properties depend not only on the properties of the reinforcement but, more importantly, on the degree to which an applied load is transferred from the matrix to the reinforcement, phenomena commonly referred as the stress transfer effect.[16,17] Then, to enhance it, the

key issues for a polymer reinforced with CNTs are the CNT dispersion, compatibilization and stabilization in the polymer matrix.[18] In this regard, a large number of reviews have been published about the functionalization of CNTs.[19–21] It covers the covalent attachment of functional moieties through reaction onto CNTs and the noncovalent adsorption or wrapping of various functional molecules to achieve a nanometric dispersion.[22–25] Chen et al.[26] has functionalized Multiwall CNTs (MWCNT) in a two-step acid-epoxy functionalization process in order to promote the covalent bonding between the f-MWCNTs and the epoxy matrix. They obtained nanocomposites with a significant enhancement in flexural strength and with similar elastic modulus. Ma et al.[27] studied the effects of silane functionalized MWCNTs on the properties of CNT-epoxy nanocomposites. They found that the grafting of silane molecules onto the CNT surface significantly improved the dispersion of MWCNTs in an epoxy matrix. Luo et al.[28] evaluated through dynamic mechanical analysis (DMA) the interfacial adhesion of MWCNTs-epoxy nanocomposites, finding that it was strongly dependent on the surface physicochemical properties of the f-MWCNTs. They used f-MWCNTs with different amino-organics (dicyanodiamide and phenylbiguanide). Other researchers have extensively studied the mechanical properties of nanocomposites based on an epoxy matrix reinforced with CNT.[29–33] However, it is important to emphasize that the effect of the physicochemical properties of the interphase on the shear induced failure of CNT nanocomposites has not been studied in depth before. Then, to evaluate the contribution of the interphase on the mechanical properties of nanocomposites, it has been hypothesized that a shear state of stress would induce an interlaminar mode of failure, which can be directly related to the interphase strength.[34] This hypothesis was directly deduced from the behavior of long fiber reinforced composites, where the most relevant testing procedure to evaluate the interlaminar failure resistance is the short-beam (SB) shear test, commonly referred as ILSS.[35,36] By reducing the span to depth ratio, it has been demonstrated that a preponderant shear state of stress could induce an interlaminar failure. It is important to notice that for the case of long fiber reinforced composites, the results of that test have become design parameters. However, this is certainly not the case for composites reinforced with fillers which have nanometric dimensions (nanocomposites). This is because, in nanocomposites, a shear induced failure mode was very difficult to obtain. In addition, taking into account that the geometry of the filler did not conform a laminate morphology, it was also expected not to have an interlaminar failure mode. However, this is certainly not the case for certain nanoparticles, such as clays and high aspect ratio carbon nanotubes, where one dimension has a micrometer scale. Then, to evaluate the ILSS of nanocomposites, modifications of the SB test have been proposed. Rodríguez-González et al.[37] proposed to modify the sample specimen by placing the nanocomposite between two metallic sheets (sandwich geometry). This helped to avoid any direct loading of the nanocomposite, which was known to induce non shear failure modes. Even though the theoretical background of the proposed approach was correct, the author did not provide any optical microscopy of the fracture surface which corroborated that the interphase had a preponderant role on the fracture phenomena. Other authors have also modified

the testing conditions, such as using a four-point flexure approach instead of a three point one.[38–40] Finally, it has been proposed that increasing the diameter of the loading nose and the support rollers could also help to induce shear failure modes.[41,42] It is important to notice that all those authors had tried to induce an interlaminar failure mode without correlating the ILSS results with fractographic analysis (evaluated with scanning electron microscopy (SEM) or transmission electron microscopy (TEM)) which could corroborate that failure mode. In addition, it can also be deduced that those authors had focus on changing only the experimental testing parameters so as to induce interlaminar failure rather than evaluating the effect of other relevant variables pertained to nanocomposites. A final objection is related to the interlaminar failure terminology. Unless the CNT or the specific nanoparticle had a significant length (within the micrometer range), it is important to notice that the failure mode cannot be denominated interlaminar, but rather, as a shear induced failure mode.

In this work, the SB testing procedure will be used to induce a shear failure mode in CNT reinforced epoxy nanocomposites. It is important to emphasize that the objective of this paper is not to evaluate a fiber reinforced composite, but rather, a nanocomposite. In addition, in contrast to what has been studied in literature, the testing procedure will not be altered. It will be demonstrated that the dispersion, functionalization and the associated failure mode of the nanocomposite are the most relevant variables to evaluate the performance under a shear state of stress. In addition, the SB results will be correlated with DMA and SEM fractographic analysis, proving that its correlation is essential to correctly evaluate the SB shear strength (SBSS) of the nanocomposites.

EXPERIMENTAL

The matrix was a diglycidylether of bisphenol-A (DGEBA) epoxy resin cured with an aliphatic amine, triethylenetetramine (TETA), both provided by Distraltec. MWCNT were purchased from Nanocyl (NC7000, Belgium). The average length of the CNT was 1.5 μm, while the external diameter was approximately 9.5 nm. This geometry contributed to a surface area of 250–300 m^2 g^{-1}. As it can be inferred, the length of the CNT can be considered to be long enough so as to have a pseudolaminar effect.

To functionalize the outer surface of the CNT, four chemical treatments were applied to the pristine CNT, from now on denominated CNT_0. An schematic representation of the theoretically expected interphase is depicted in Figure 1. The first chemical treatment, referred as CNT_1, consisted on the thermal oxidation of the CNT_0. This was performed in an oven at 400°C for 8 h. Taking into account that a prolonged heat treatment could induce a relevant structural modification of the CNT walls, SEM micrographs were used so as to corroborate that no substantial changes were induced. It was found that 8 h was the appropriate time which generated a sufficient amount of reactive groups on the CNT surface while not deteriorating the CNT geometrical integrity.[43] The second chemical treatment (CNT_2) consisted on the silanization of the carboxylic and hydroxide groups present on the surface of the CNT_1 type. The
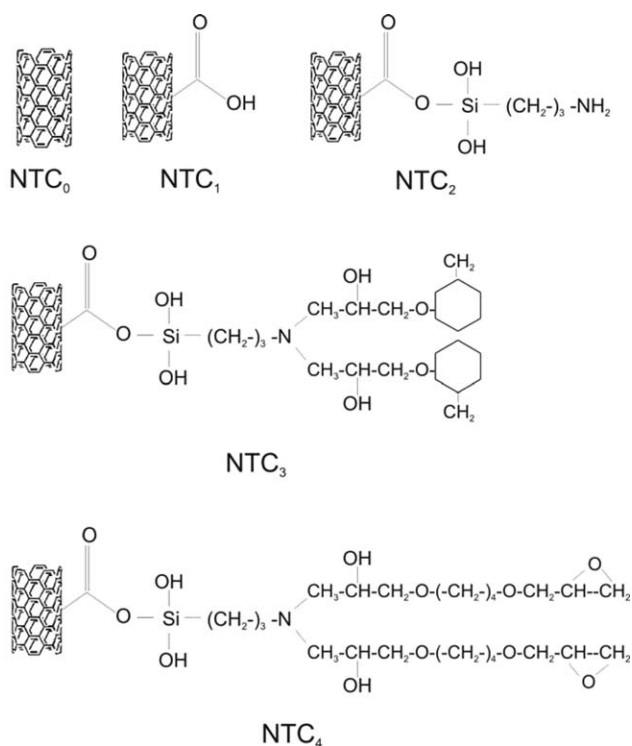
Figure 1. Schematic representation of the f-CNT.

silanization method was based on the anhydrous liquid phase deposition method.[44] During the reaction, 50 mg of CNT_1 were first dispersed in 30 mL of isopropanol (Sigma-Aldrich) using an ultrasonic mixer (Testlab TB02TA, at 200 W) for 1 h. Afterward, 3 mL of aminopropyltriethoxysilane (APTS, Sigma-Aldrich) was added and the reaction temperature was increased to 70°C, maintaining that temperature for 8 h. For the entire reaction time, the solution was mixed with a magnetic stirrer at 500 rpm. Afterwards, the liquid mixture was filtered and washed with a nylon membrane filter (MS®, pore size 0.22 μm) using 500 mL of Deionized (DI) water (18.2 MΩ) and 100 mL acetone (Sigma-Aldrich). Then, the filtered powder was dried in a vacuum oven overnight (80°C, 40 mbar). The third chemical treatment (CNT_3) was based on the formation of an extended CNT outer layer by using the chemical reaction between ortho-cresylglycidylether (OCGE) and the outer surface groups of the CNT_2 (secondary amine type radicals). During the reaction, 22.8 mg of CNT_2 were ultrasonically mixed in 100 mL of methyl ethyl ketone (MEK) for 1 h. Subsequently, the temperature was set to 60°C and 3 mL of OCGE were added to the solution. Then, the reaction proceeded at isothermal conditions (60°C) for 12 h. When the reaction ended, the CNT_3 was vacuum filtered (identical membrane described above) and washed with 500 mL of DI water (18.2 MΩ). Finally, the filtered powder was dried in a vacuum oven overnight (60°C, 40 mbar). The fourth chemical treatment (CNT_4) consisted on the extension of the CNT outer layer by means of the chemical reaction between the outer surface groups of the CNT_2 and 1–4, butanedioldigly-cidylether (DGEBD). To achieve this, 17.2 mg of CNT_2 were initially ultrasonically mixed for an hour in a solution of 50 mL of MEK. Subsequently, the temperature was set to 60°C and 1.1 mL of DGEBD was added to the solution. Then, the reac-

tion proceeded at isothermal conditions for 12 h. When the reaction ended, the CNT_4 was filtered and washed with 500 mL of DI water (18.2 MΩ). The filtered powder was vacuum dried in an oven overnight (60°C, 40 mbar).

As far as the preparation of the composites is concerned, the dispersion of all CNT used in this work was performed in the DGEBA monomer. The procedure consisted in setting up a beaker with 20 g of DGEBA with a batch temperature of 80°C. Subsequently, 22.5 mg of CNT_i was added (the subindex i denotes either 0, 1, 2, 3, or 4). Afterwards, the ultrasonic mixer (Testlab TB02TA) and the homogenizer (Bio-Homogenizer Pro 200Gen) were activated. The ultrasonic mixer was set to the maximum power (200 W) while the homogenizer rotated at 5000 rpm. This combined dispersion process lasted 1 h. After this, the CNT_i dispersed in DGEBA was vacuum mixed for 30 min. so as to remove entrapped bubbles. Then, 2.5 g of TETA were added and manually mixed for 3 min. Finally, the resin was poured in an open glass mould with dimensions of 200 mm in length, 150 mm in width and 2 mm thick. Finally, the glass mould was introduced in a furnace oven and cured following a specific temperature program of three isothermal stages. The first one lasted 2 h at 40°C, the second one 2 h at 120°C and the last one 2 h at 140°C. In this work, a fixed concentration of CNT was implemented, that is, 0.1 wt % (0.08 vol %). It is not the objective of this publication to study the effect of concentration, information about that effect can be consulted elsewhere.[45] In addition, the weight relationship between DGEBA and TETA was calculated so as to have an stoichiometric ratio. In other words, all the epoxide groups reacted with amine groups to conform a crosslinked network.

Thermal degradation of the CNT was performed using a thermogravimetric analyzer (Shimadzu TGA 50). The thermal experiment consisted of a thermal scan at a velocity of 10°C min^{-1} from 30°C up to 800°C. The infrared absorption spectrum of the CNT_i was performed using a Shimadzu IRAffinity-1. The attenuated total reflection (ATR) methodology was used to achieve that (Shimadzu, ATR-8200HA) purpose. A ZnSe prism with and incidence angle of 45° was used. DMA was performed with a Perkin & Elmer DMA 8000. The single cantilever bending mode was used, with an oscillation frequency of 1.0 Hz and amplitude of 0.05. The thermal scan started at 30°C and went up to 180°C with a scan rate of 2°C min^{-1}. The SB shear test (SBSS) was performed by means of a Universal Testing Machine (Lloyd Instruments LR30K) at a velocity of 1 mm min^{-1} a span of 8 mm and sample dimensions of 2.7 mm in thickness and 4.55 mm in width. It should be noticed that the previous parameters followed the guidelines of the standard ASTM 2344. SEM micrographs were obtained with a ZEISS field emission scanning electron microscope model Supra 25. Each sample obtained after SBSS failure were metalized with a thin layer of gold (15 nm, 99.99% Au at 2.10^{-6} Torr.) using the physical vapor deposition technique. For the surface analysis, secondary electrons were used.

It should be noticed that, in this work, the term ILSS will be used for the evaluation of the ILSS of long fiber composites. In contrast, the term SBSS will be used for the evaluation of the
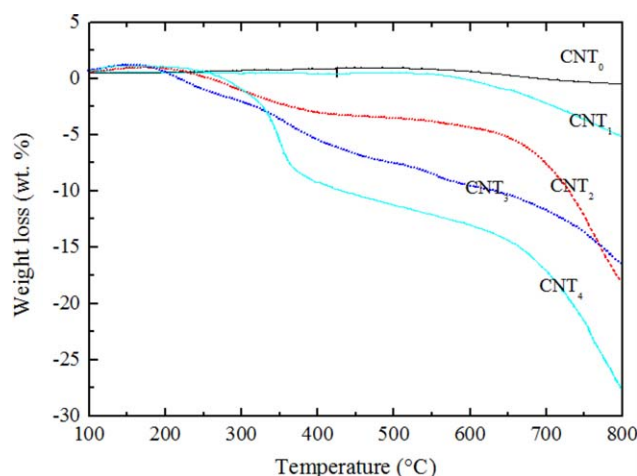
Figure 2. Weight loss as a function of temperature for the f-CNT. [Color figure can be viewed in the online issue, which is available at wileyonline-library.com.]

SBSS of the nanocomposites. As it can be deduced, even though a different nomenclature has been used, the experimental procedures to obtain those results were identical.

RESULTS AND DISCUSSION

Interphase Characterization

The thermal stability of the CNT, measured as weight loss as a function of temperature, is depicted in Figure 2. For the case of the CNT_0, an almost null weight loss was found within the temperature range 30–700°C. Taking into account that no organic phase was present on the CNT_0, this result was to be expected. Similarly, the CNT_1 showed a slight weight loss within the temperature range 30–700°C. This indicated that the oxidation treatment removed most of the amorphous carbon, leading to an improved thermal stability up to 750°C. It should be noticed that the previous results were in agreement with has already been published.[46,47]

In contrast, for the case of the CNT synthesized with an organic interphase (CNT_2, CNT_3 and CNT_4), the weight loss was significant. Specifically, the weight fraction of organic interphase at 600°C was 4.5 wt % for CNT_2, 10 wt % for CNT_3, and 13.4 wt % for CNT_4. From these values, it can be deduced that the thickness of the organic interphase increased in the following order: $CNT_4 > CNT_3 > CNT_2$. Then, it can be inferred that the experimental results were in agreement with what was theoretically expected (Figure 1).[48]

Even though the TGA analysis proved that the organic interphase was present on the f-CNT, Fourier transform-infrared analysis was performed so as to corroborate that the organic interphase was present and covalently bonded to the outer surface of the f-CNT. The absorption spectra of the f-CNT are shown in Figure 3. On the left side of Figure 3, it is presented the spectra from a wavelength interval of 3700 to 2700 cm^{-1}, while in the right side, the wavelength interval 1800–800 cm^{-1} is shown. It should be noted that the absorptions centered at 2917 and 2847 cm^{-1} can be ascribed to the ─CH stretching mode of the CNTs backbone and/or the epoxy backbone struc-

ture, which are present in all spectra. Moreover, the absorption intensity of those vibrations increased for samples which contained the grafted epoxy groups. On the other hand, the broad absorption band at 3433 cm^{-1} was associated to the ─OH stretching vibration present in the different functionalized states (Figure 1). The absorption band at 1631 cm^{-1} was assigned to the conjugated C═C stretching mode. On the other hand, the CNT_1 spectra presented a band at 1722 cm^{-1} which can be assigned to the C═O stretching vibration of carboxyl groups.[49] In addition, the CNT_3 and CNT_4 samples presented an absorption band at 870 cm^{-1}, which was associated to the presence of epoxy groups on the CNT surface.[50] Moreover, the absorption band at 1461 cm^{-1} corresponded to the stretching mode of NH groups.[51] Another absorption band at 1395 cm^{-1} corresponded to the in-plane OH deformational vibration of ─COOH groups. The absorption bands in the region 1000–1200 cm^{-1} were ascribed to the presence of additional vibration modes associated to Si─O, Si─C, and Si─OH groups.[46] In summary, the absorption spectra of the f-CNT corroborated that the organic interphase was present and covalently bonded to the outer surface of the CNT.

SBSS and Fractography of the Nanocomposites

The results of the SB test (SBSS) as a function of CNT functionalization are reported in Table I. Then, it could be inferred that the SBSS results changed as a function of CNT functionalization. As it was said before, it is of utmost importance to evaluate the fractographic behavior associated with the SB test results.

The fracture surface of an epoxy composite with 0.1 wt % of CNT_0 is shown in Figure 4. The main features that can be distinguished at low magnification were detached particles [Figure 4(a)], isolated and agglomerated CNT [Figure 4(b)] and the fracture surface texture. An important amount of detached particles with dimensions in the order of 1–10 μm were found, indicating that the reinforcement effect of the CNT_0 did not affect the fragile nature of the epoxy matrix (absence of the stress transfer effect). This was further confirmed with the fracture surface, which was found to be almost independent of the presence of CNT_0. In fact, as it is shown in Figure 4(b), the crack propagation path was not dependent on the presence of the CNT_0. Moreover, the distribution of the CNT_0 in the matrix was mainly in the shape of agglomerates. Two different types of agglomerates were found. The first one was composed of a very dense distribution of CNT_0 [Figure 4(b)] while the second type was composed of CNT which were distributed in an almost exfoliated way [Figure 4(c,d)].

The fracture surface of an epoxy nanocomposite with 0.1 wt % of CNT_1 is shown in Figure 5. The main features that can be distinguished at low magnification [Figure 5(a)] were detached particles, CNT_1 agglomerates and the fracture surface texture. An important amount of detached particles with dimensions of less than 1 μm were found. In contrast to CNT_0, those particles took part of the formation of the texture of the fracture surface, indicating that the CNT_1 had a more relevant role in modifying the fracture behavior of the epoxy matrix (strong stress transfer effect). Particularly, the planes where the crack propagated
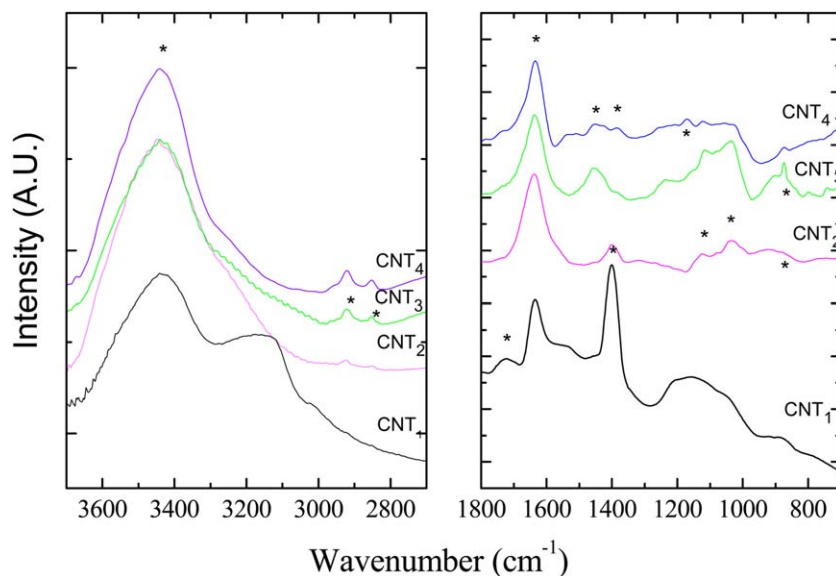
Figure 3. Infrared absorption spectra of the f-CNT. The left figure shows the wavenumber interval 3600-2800 cm^{-1} while the right figure shows the wavenumber interval 1800–800 cm^{-1}. [Color figure can be viewed in the online issue, which is available at wileyonlinelibrary.com.]

clearly depended on the CNT_1 distribution. As is it shown in Figure 5(b), a shift of the propagation path was clearly induced by the CNT_1. Taking into account the SEM micrographs shown in Figure 5(b,c), it can be deduced that the crack propagated inside the outer area of the agglomerate, where the density of CNT_1 was low and, subsequently, it was constricted to change the propagation plane due to the high energy associated to the area increase. Another important aspect that has to be noted is that in the region where the crack propagation plane shifted, the CNT_1 were not pulled apart from the matrix, indicating a strong interphase and a substantial stress transfer effect.

The fracture surface of an epoxy nanocomposite with 0.1 wt % of CNT_2 is shown in Figure 6. The main features that can be distinguished at low magnification [Figure 6(a)] were CNT_2 agglomerates and the fracture surface texture. Most of the CNT_2 was dispersed in an agglomerate morphology with dimensions in the order of 10 μm. These agglomerates were arranged by a compact and dense distribution of CNT_2, surrounded by some exfoliated CNT_2. As far as the correlation between the fracture surface and the presence of the CNT_2, the fracture behavior was not substantially modified by the presence of the CNT_2. In fact, as it is shown in Figure 6(c), the crack propagated over the outer area of the CNT_2 agglomerate but stopped after reaching the core. Then, it can be inferred that the CNT_2 behaved as a micrometric reinforcement, because the

contact area of the CNT_2 agglomerates with the epoxy matrix was not elevated (absence of stress transfer effect).

The fracture surface of an epoxy nanocomposite with 0.1 wt % of CNT_3 is shown in Figure 7. The main features that can be distinguished, at low magnification [Figure 7(a)], were CNT_3 agglomerates and the fracture surface texture. The agglomerates were found to have very heterogeneous dimensions which fell within the range 0.1–10 μm and with a structure composed by a dense array of CNT_3. In contrast to the CNT_2, the compact agglomerates contributed substantially to the formation of the texture of the fracture surface. In fact, as it is shown in Figure 7(a), the propagation of the crack was clearly influenced by the presence of the CNT_3 agglomerate. Specifically, when the crack propagated to the surroundings of the CNT_3 agglomerate, it tended to change the propagation plane more frequently. In addition, when the crack propagated inside the agglomerate, this tendency was further intensified [Figure 7(c)]. Then, it can be inferred that, in contrast to the CNT_2, the CNT_3 contributed to a stronger stress transfer between matrix and filler.

The fracture surface of an epoxy nanocomposite with 0.1 wt % of CNT_4 is shown in Figure 8. The main features that can be distinguished, at low magnifications [Figure 8(a)], were CNT_4 agglomerates and the fracture surface texture. The agglomerates were found to have dimensions which fell in the range 1–10 μm. Very compact and dense agglomerates were found dispersed in the epoxy matrix, nevertheless, a strong stress transfer effect was also taking place. This affirmation is supported by the way in which the crack growth was affected by the presence of the CNT_4 agglomerates, which is clearly depicted in Figure 8(b,c). Moreover, defects were found surrounding the CNT_4 agglomerates [Figure 8(c)]. Then, it can be concluded that, from a fracture point of view, the CNT_4 behaved similarly to the CNT_3.

As already stated above, the SBSS results depended on the surface functionalization of the CNT (Table I). From the obtained results, it can be deduced that the surface functionalization

Table I. SB Shear Strength as a Function of Epoxy-CNT Type

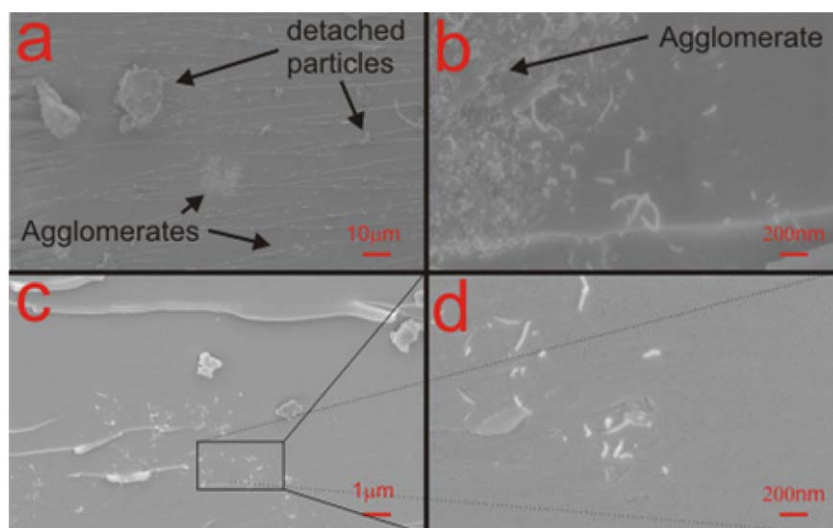| Nanocomposite	SBSS (Mpa)	Fractional variation (%)
Epoxy-CNT$_0$ 0.1 wt %	22.1 ± 1.44	0 (baseline)
Epoxy-CNT$_1$ 0.1 wt %	22.1 ± 1.60	0.00 ± 9,74
Epoxy.CNT$_2$ 0.1 wt %	24.5 ± 1.14	+10.9 ± 8.90
Epoxy-CNT$_3$ 0.1 wt %	18.3 ± 1.72	−17.2 ± 9.47
Epoxy-CNT$_4$ 0.1 wt %	22.7 ± 1.31	+2.71 ± 8.94

Figure 4. Fracture surface of an epoxy-CNT_0 0.1% wt at a) low magnification (2.5k×), showing detached particles and CNT_0 agglomerates and b) magnified agglomerate of section a. c) Section without CNT_0 agglomeration and d) magnified version of section c. [Color figure can be viewed in the online issue, which is available at wileyonlinelibrary.com.]

could induce a neutral, positive or detriment effect on the SBSS. The neutral effect can be associated to the nanocomposites prepared with CNT_0 and CNT_1 while the positive effect to the CNT_3 and CNT_4 ones and, finally, the detrimental effect to the CNT_2 one. As far as the neutral effect is concerned, it is relevant to notice that the surface functionalization of the CNT_0 contributed to the formation of an interphase which was not covalently bonded to the matrix. Then, it was expected to have a neutral effect on the SBSS results. Taking into account that the fractographic results showed no modification of the fracture surface, it can be deduced that the nanocomposite prepared with CNT_0 would not induce an improvement of the SBSS. In contrast, the nanocomposite prepared with CNT_1 had an interphase which was covalently bonded to the matrix through a ring opening reaction between the epoxy group and the carboxyl group present on the surface of the CNT_1.[52] From a fractographic point of view, the CNT_1 contributed to the formation

of the fracture surface, however, those changes were not translated into an improvement of the SBSS performance.

As far as the detriment effect is concerned, the nanocomposites prepared with CNT_2 presented the lowest SBSS values. Taking into account the CNT_2 functionality (Figure 1), it was expected to have a strong chemical interaction with the epoxy matrix. It is known that primary amine groups react with epoxide groups through and addition type reaction.[53] As a matter of fact, it was expected that the primary amine groups left after the CNT compatibilization treatment would react with the epoxy monomer before cure. This would contribute to the formation of compact CNT_2 agglomerates which would be colloidally dispersed in the epoxy monomer before cure. Assuming that all amine type groups reacted, then it can be inferred that the CNT_2 agglomerates could not form an additional covalent bond with the epoxy matrix when the cure agent was added (TETA).
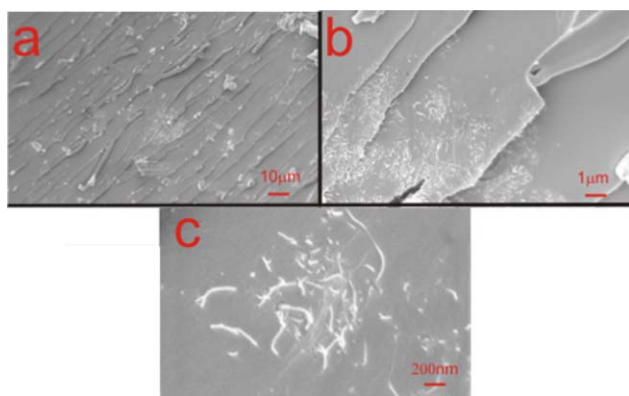

Figure 5. Fracture surface of an epoxy-CNT_1 0.1% wt at a) low magnification (2.5k×), showing detached particles and CNT_1 agglomerates with its subsequent magnifications (sections b and c). [Color figure can be viewed in the online issue, which is available at wileyonlinelibrary.com.]
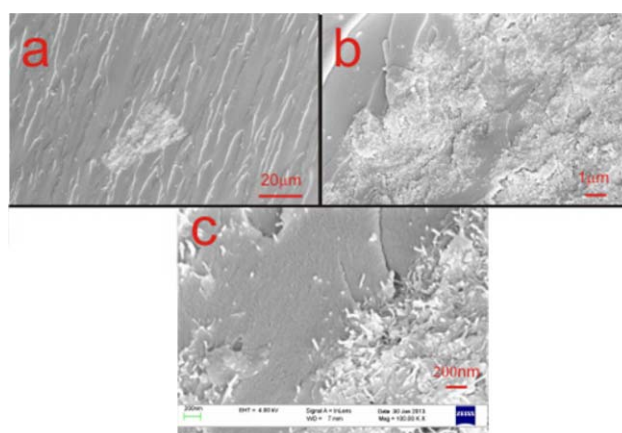

Figure 6. Fracture surface of an epoxy-CNT_2 0.1% wt at a) low magnification (2.5k×) showing detached particles and CNT_2 agglomerates with its subsequent magnifications (sections b and c). [Color figure can be viewed in the online issue, which is available at wileyonlinelibrary.com.]
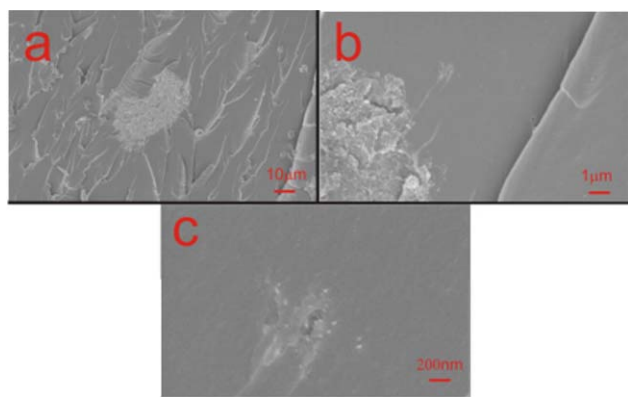
Figure 7. Fracture surface of an epoxy-CNT_3 0.1% wt at a) low magnification (2.5k×) showing detached particles and CNT_3 agglomerates with its subsequent magnifications (sections b and c). [Color figure can be viewed in the online issue, which is available at wileyonlinelibrary.com.]

From this, it can be deduced that the agglomerates were internally connected through covalent bonds but not covalently bonded to the bulk. Then, even though the initial surface functionality could infer a strong covalent interaction with the epoxy matrix, this was not certainly the case because of the agglomeration caused before cure. This conclusion is corroborated by both the SBSS and the fractographic results. As it was showed before, the lowest SBSS value was obtained with the CNT_2 (Table I) nanocomposite and a strong agglomeration without matrix interaction was observed with SEM micrographs (Figure 6). Another side effect of the CNT_2 functionalization was related to a change of the stoichiometric ratio during cure. This would also contribute to a deterioration of the SBSS performance.

Finally, an improvement of the SBSS performance was obtained with the nanocomposites prepared with CNT_3 and CNT_4. For the case of the nanocomposites prepared with CNT_3, the functionalization contributed to the formation of the hindrance effect, described by Montazeri.[54] In addition, the functionality prevented a change of the stoichiometric ratio during cure. Both aspects were associated to the improvement of the SBSS
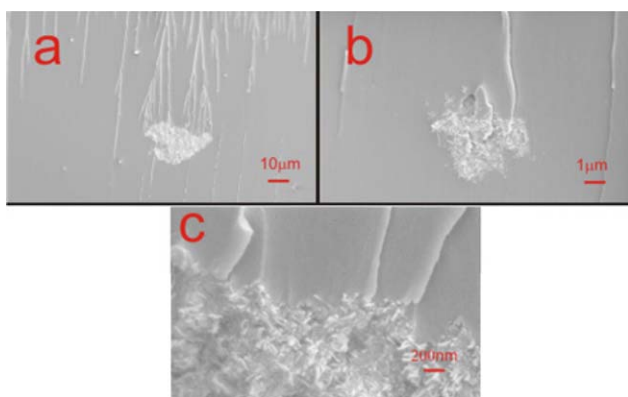
performance. As far as the nanocomposites prepared with CNT_4 is concerned, it was expected to have the strongest covalent interaction with the matrix. This was because the epoxide group present in the CNT_4 would react with the TETA during cure (ring opening reaction). However, even though the SBSS performance was among the highest, it was not the best. This behavior can be explained based on the fractographic analysis and the stoichiometric ratio. Taking into account that the CNT_4 added epoxy groups in the monomer, the epoxy equivalent increased. Then, unreacted epoxy after cure would cause a plasticizer effect. Furthermore, taking into account that the CNT_4 can be considered as an epoxy monomer with a different backbone, it was expected to have a modification of the cure kinetics. A local change of the cure kinetics would cause regions with dissimilar cure shrinkage. Evidence of this hypothesis was found in the fractographic analysis (Figure 8), where defects were encountered on the surroundings of the CNT_4 agglomerates.

Dynamic Mechanical Thermal Analysis of the Nanocomposites

The effect of CNT functionalization on the storage modulus (E') of an epoxy matrix reinforced with CNT (0.1 wt %) is shown in Figure 9. It is important to emphasize that the discussion will be centered on the properties of the epoxy-CNT nanocomposite and, whenever a reference is made to a specific CNT functionalization, it will implicitly refer to the behavior of the epoxy-CNT nanocomposite. As far as the E' on the glassy region is concerned, from Figure 9 it can be deduced that the functionalization of the CNT had a negligible effect on its value (the numerical values are reported in Table II). It should be noticed that, taking into account the concentration of CNT used, this result was to be expected. The load transfer was probably caused between the outer most layer of multiwall nanotubes and the epoxy matrix, resulting in a much lower effective content of reinforcing nanotubes, in accordance with other authors.[55,56] At intermediate temperature, the functionalization of the CNT started to show a relevant role. As a matter of fact, fixing an E' value within the glass to rubbery transition, the
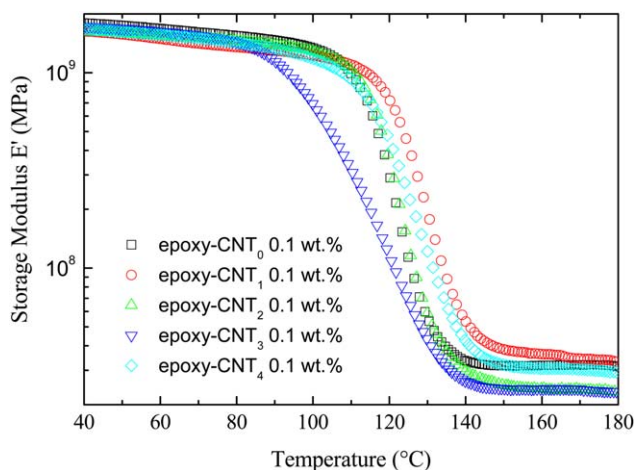

Figure 8. Fracture surface of an epoxy-CNT_4 0.1%wt at a) low magnification (2.5k×) showing detached particles and CNT_4 agglomerates with its subsequent magnifications (sections b and c). [Color figure can be viewed in the online issue, which is available at wileyonlinelibrary.com.]

Figure 9. The effect of CNT functionalization on the Storage Modulus (E') of epoxy-CNT at 0.1 wt %. [Color figure can be viewed in the online issue, which is available at wileyonlinelibrary.com.]

Table II. Summary of DMA Properties of the Epoxy-CNT Nanocomposites

Material	$E'_{40°C}$ (MPa)	$T_{Tan\,\delta}$ (°C)	$|Tan\,\delta|$	$E'_{160°C}$ (MPa)
Epoxy-CNT$_0$ 0,1 wt %	$1.80 \times 10^2 \pm 5.1$	$1.25 \times 10^2 \pm 9.1$	$6.6 \times 10^{-1} \pm 0.02$	$3.17 \times 10^1 \pm 6.1$
Epoxy-CNT$_1$ 0,1 wt %	$1.63 \times 10^2 \pm 4.3$	$1.33 \times 10^2 \pm 11.1$	$5.2 \times 10^{-1} \pm 0.03$	$3.63 \times 10^1 \pm 5.4$
Epoxy-CNT$_2$ 0,1 wt %	$1.62 \times 10^2 \pm 6.1$	$1.26 \times 10^2 \pm 8.7$	$7.4 \times 10^{-1} \pm 0.04$	$2.38 \times 10^1 \pm 3.4$
Epoxy-CNT$_3$ 0,1 wt %	$1.72 \times 10^2 \pm 3.6$	$1.23 \times 10^2 \pm 12.3$	$3.4 \times 10^{-1} \pm 0.06$	$2.40 \times 10^1 \pm 6.1$
Epoxy-CNT$_4$ 0,1 wt %	$1.67 \times 10^2 \pm 4.8$	$1.31 \times 10^2 \pm 7.6$	$4.3 \times 10^{-1} \pm 0.08$	$3.04 \times 10^1 \pm 7.3$

temperature decreased in the following order: $T_{CNT1} > T_{CNT4} \approx T_{CNT2} \approx T_{CNT0} > T_{CNT3}$. On the other side, the E' above the glass to rubbery transition (T > 140°C) was strongly dependent on CNT functionalization (Table II). As a matter of fact, the E' increased as a function of CNT functionalization following this order: $E'_{CNT1} > E'_{CNT0} \approx E'_{CNT4} > E'_{CNT2} \approx E'_{CNT3}$.

DMA was also used to evaluate the effect of CNT functionality on the crosslinking density, through the calculation of the cross-link molecular weight (M_c). This value was determined using the following equation[57]:

$$E' = \frac{3\rho RT}{M_c} \quad (1)$$

where E' represents the storage modulus in the rubbery plateau region, R is the Boltzmann constant, T is the temperature, and ρ is the sample density.

From the results (Table III) it can be deduced that the highest value of M_c was for the epoxy-CNT$_2$ nanocomposite. In addition, the M_c decreased in the following order: $M_{cCNT2} > M_{cCNT3} > M_{cCNT4} > M_{cCNT0} > M_{cCNT1}$. This behavior can be explained by taking into account the length and nature of the interphase. The CNT$_2$ had an amine-terminal group and represented the highest reactive functional group with respect to the epoxy group. During the preparation of the nanocomposites, each type of CNT was dispersed initially in the DGEBA precursor with the aid of sonication (more details were explained in the experimental section above). When the catalyst was being incorporated, the epoxy group which reacted with the amine-terminal group from the CNT surface modified the stoichiometry and lead to an opened network and a consequently higher M_c.

In contrast, the nanocomposites containing CNT$_3$ and CNT$_4$ had a lower M_c. Both nanocomposites contained the largest interphase which included the OCGE and the DGEBD functional groups. Both systems had a highly negative electronic density which gave place to strong repulsive forces, allowing a better dispersion of the CNT after the preparation of the nanocomposite (hindrance effect). Then, it can be deduced that the incorporation of this kind of nanofiller increased the amount of spacing between crosslinks.[58] This could explain the high value of the M_c for those samples.

Finally, the most compact network corresponded to the epoxy-CNT$_1$ nanocomposite. This could indicate that the dispersion of the CNT$_1$ was better than the other cases. The carboxyl group on the CNT$_1$ surface probably reacted with the epoxy group of the precursor through ring opening reaction. This contributed to the formation of a strong covalent bond during the disper-

sion stage. This deduction can also be correlated with the SEM fracture analysis. As already stated in the previous section, the fracture surface was substantially modified by the presence of the CNT$_1$, indicating a strong stress transfer effect. Contrasting this observation with the DMA results, it can be inferred that the strong transfer effect can be associated with the value of E' above the T_g. In addition, contrasting this deduction with the results of Rahman et al.[59], it can be deduced that the functionalization of the CNT lead to a decrease in the E', implying an increase of the flexibility of the nanocomposite. Montazeri et al.[60] reported that, in the rubbery state, the molecular motion and its amplitude remained elevated and the macromolecule was essentially without contact with the filler, with no shear force acting among them.

In the previous paragraphs, only the elastic response was analyzed. To further understand the dynamic behavior of the composite, the tan δ (damping factor) as a function of temperature and the CNT functionalization is depicted in Figure 10. The results showed that the CNT functionalization had a strong effect on the damping factor. Specifically, for the case of the epoxy-CNT$_3$ composite, the full width at half maximum of damping factor increased significantly, indicating that the viscous component of the composite was significant even for low temperatures ($T\sim80°C$). In addition, the maximum damping factor for each nanocomposite can be correlated to the SBSS performance. As it was shown before, the highest SBSS performance was associated to the epoxy-CNT$_3$ nanocomposite. Furthermore, as it is shown in Table II, the lowest damping factor was also associated to the epoxy-CNT$_3$ nanocomposite. In contrast, the lowest ILSS performance was associated to the epoxy-CNT$_2$ nanocomposite, which also had the highest damping factor Table II. To furtherly corroborate this tendency; a linear fitting was elaborated between the SBSS and the damping factor results. If the values associated with the epoxy-CNT$_0$ are omitted, a linear regression was obtained ($R^2 = 0.97$). Then, it can be concluded that the damping factor was correlated to the

Table III. Calculated M_c as a Function of Epoxy-CNT Type

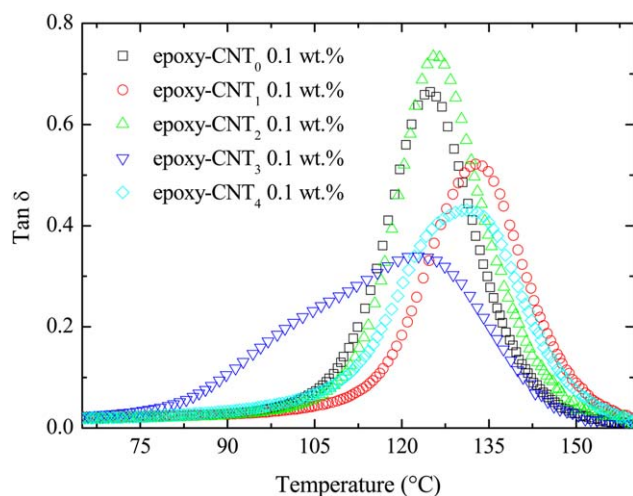| Nanocomposite	M_c (g mol^{-1})
Epoxy-CNT$_0$ 0.1 wt %	$6.05 \times 10^{-1} \pm 0.005$
Epoxy-CNT$_1$ 0.1 wt %	$5.28 \times 10^{-1} \pm 0.003$
Epoxy.CNT$_2$ 0.1 wt %	$8.06 \times 10^{-1} \pm 0.001$
Epoxy-CNT$_3$ 0.1 wt %	$7.99 \times 10^{-1} \pm 0.01$
Epoxy-CNT$_4$ 0.1 'wt %	$6.31 \times 10^{-1} \pm 0.009$

Figure 10. The effect of CNT functionalization on damping factor (Tan δ) for CNT reinforced epoxy nanocomposites at 0.1 wt %. [Color figure can be viewed in the online issue, which is available at wileyonlinelibrary.com.]

ILSS performance after the functionalization effect was taken into consideration. This is an additional fact which supports the hypothesis that the CNT surface functionalization is a much more relevant variable instead of the change of the testing conditions.

CONCLUSIONS

MWCNT were effectively functionalized with different functional groups obtaining a high coverage degree (up to 30 wt %). Hydroxide, amino, and epoxy groups were used to functionalize CNT. The influence of the CNT surface functionalization on the SBSS was substantial. In fact, a positive (up to 10.9%±8.9), neutral and detrimental (down to −17.2%±9.5) effect was measured as a function of functionalization. The positive effect, associated to epoxy reinforced with CNT_3 and CNT_4, had a fracture surface which indicated a strong stress transfer effect. The neutral effect, associated to epoxy reinforced with CNT_0, had a SEM fracture surface which indicated that the CNT_0 did not contribute to a stress transfer effect. Finally, the detrimental effect, associated to epoxy reinforced with CNT_2, had a SEM fracture surface which indicated the presence of big agglomerates (10 μm) with no stress transfer effect. The validity of the SBSS results was associated to the presence of the stress transfer effect. The absence of this effect indicated that the nanofiller did not contribute to the induction of a shear failure mode.

In addition, these results were correlated to the DMA analysis. The epoxy-CNT_3 had the highest SBSS value and the lowest |Tan δ|. In contrast, the epoxy-CNT_2 had the lowest SBSS and the highest |Tan δ|. Then, it can be inferred that a strong correlation among CNT surface functionalization, SEM fractography and DMA was obtained.

REFERENCES

1. Zhang, X.; Hounslow, L.; Grassi, M. *Compos. Sci. Technol.* **2006**, *66*, 2785.

2. Byrd, L. W.; Birman, V. *Compos. Part B: Eng.* **2006**, *37*, 365.

3. Partridge, I. K.; Cartie, D. *Compos. Part A: Appl. Sci. Manuf.* **2005**, *36*, 55.

4. Yokozeki, T.; Iwahori, Y.; Ishiwata, S. *Compos. Part A: Appl. Sci. Manuf.* **2006**, *38*, 917.

5. Shahid, N.; Villate, R.; Barron, A.R. *Compos. Sci. Tech.* **2005**, *65*, 2250.

6. Siddiqui, N. A.; Woo, R. S.; Kim, J. K.; Leung, C. C.; Munir, A. *Compos. Part A: Appl. Sci. Manuf.* **2006**, *38*, 449.

7. Yan, S.; Yin, J.; Cui, L.; Yang, Y; Chen, X. *Colloids Surf B: Biointerfaces* **2011**, *86*, 218.

8. Fan, Z. H.; Santare, M. H.; Advani, S. G. *Compos. Part A: Appl. Sci. Manuf.* **2008**, *39*, 540.

9. Miyagawa, H.; Jurek, R. J.; Mohanty, A. K.; Misra, M.; Drzal, L. T. *Compos. Part A*, **2006**, *37*, 54.

10. Li, F.; Lu, Y.; Liu, L.; Zhang, L.; Dai, J.; Ma, J. *Polymer* **2013**, *54*, 2158.

11. Thostenson, E. T.; Chou, T. W. *Carbon* **2006**, *44*, 3022.

12. Zhuang, R. C.; Doan, T. T.; Liu, J. W.; Gao, S. L.; Mäder, E. *Carbon* **2011**, *49*, 2683.

13. Ghaleb, Z. A.; Mariatti, M.; Ariff, Z. M. *Compos. Part A: Appl. Sci. Manuf.* **2014**, *58*, 77.

14. Rahman, M. M.; Zainuddin, S.; Hosur, M. V.; Robertson, C. J.; Kumar, A.; Trovillion, J.; Jeelani, S.; *Compos. Struct.* **2013**, *95*, 213.

15. Wichmann, M. H. G.; Sumfleth, J.; Gojny, F. H.; Quaresimin, M.; Fiedler, B.; Schulte, K. *Eng. Fract. Mech.* **2006**, *73*, 2346.

16. Zheng, Q. B.; Xue, Q. Z.; Yan, K. Y.; Gao, X. L.; Li, Q.; Hao, L. Z. *Polymer* **2008**, *49*, 800.

17. Ma, P.; Zheng, Q.; Mäder, E.; Kim, J. *Polymer* **2012**, *53*, 6081.

18. Terenzi, A.; Vedova, C.; Lelli, G.; Mijovic, J.; Torre, L.; Valentini, L.; Kenny, J. *Compos. Sci. Tech.* **2008**, *68*, 1862.

19. Meng, L.; Fu, C.; Lu, Q. *Prog. Nat. Sci.* **2009**, *19*, 801.

20. Ma, P.; Siddiqui, N.; Marom, G.; Kim, J. *Compos. Part A: Appl. Sci. Manuf.* **2010**, *41*, 1345.

21. Polo-Luque, M. L.; Simonet, B. M.; Valcárcel, M. *Trends Anal. Chem.* **2013**, *47*, 99.

22. Ran, M.; Sun, W.; Liu, Y.; Chu, W.; Jiang, C. *J. Solid State Chem.* **2013**, *197*, 517.

23. Kasperski, A.; Weibel, A.; Estournès, C.; Laurent, C.; Peigney, A. *Scr. Mater.* **2014**, *75*, 46.

24. Ghosh, A.; Rao, K.; Voggu, R.; George, S. *Chem. Phys. Lett.* **2010**, *488*, 198.

25. Petrie, K.; Docoslis, A.; Vasic, S.; Kontopoulou, M.; Morgan, S.; Z. Ye. *Carbon* **2011**, *49*, 3378.

26. Chen, W.; Auad, M.; Williams, R.; Nutt, S. *Eur. Polym. J.* **2006**, *42*, 2765.

27. Ma, P.; Kim, J.; Tang, B. *Compos. Sci. Technol.* **2007**, *67*, 2965.

28. Luo, Y.; Zhao, Y.; Cai, J.; Duan, Y.; Du, S. *Mater. Des.* **2012**, *33*, 405.

29. Montazeri, A.; Chitsazzadeh, M. *Mater. Des.* **2014**, *56*, 500.

30. Ogasawara, T.; Moon, S; Inoue, Y.; Shimamura, Y. *Compos. Sci. Technol.* **2011**, *71*, 1826.

31. Gallego, M.; Bernal, M.; Hernandez, M.; Verdejo, R.; Lopez-Manchado, M. A. *Eur. Polym. J.* **2013**, *49*, 1347.

32. Koo, J. In Polymer Nanocomposites: Processing, Characterization, and Applications; Mcgraw-Hill Nanoscience and Technology Series: New York, **2006**; Chapter *3*, p 30.

33. Esposito, C. C.; Freuli, F.; Maffezzoli, A. *Polym. Eng. Sci.* **2013**, *53*, 1548.

34. Wan, H.; Delale, F.; Shen, L. *Mech. Res, Commun.* **2005**, *32*, 481.

35. Zhihang, F.; Santare, M.; Advani, S. *Compos. Part A: Appl. Sci. Manuf.* **2008**, *39*, 540.

36. Yokozeki, T.; Iwahori, Y.; Ishibashi, M.; Yanagisawa, T.; Imai, K.; Arai, M.; Takahashi, T.; Enomoto, K. *Compos. Sci. Technol.* **2009**, *69*, 2268.

37. Rodríguez-González, J. A.; Avilés, F. *Polym. Test.* **2012**, *31*, 792.

38. Abali, F.; Pora, A.; Shivakumar, K. J. *Compos. Mater.* **2003**, *37*, 453.

39. Rahhal, W. F.; Kotlensky, W. V. *Carbon* **1992**, *30*, 385.

40. Cui, W. C.; Wisnom, M. R. *Compos. Sci. Technol.* **1992**, *45*, 323.

41. Rahhal, W. F.; Kotlensky, W. V. *Carbon* **1992**, *30*, 385.

42. Abali, F.; Pora, A.; Shivakumar, K. *J. Compos. Mater.* **2003**, *37*, 453.

43. Kim, J. A.; Seong, D. G.; Kang, T. J.; Youn, J. R. *Carbon* **2006**, *44*, 1898.

44. Gelest, I. Silane coupling agents: Connecting accross boundaries. Available at: www.gelest.com (accessed on October 20, 2013).

45. Gojny, F.; Schulte, K. *Compos. Sci. Technol.* **2004**, *64*, 2303.

46. Miyagawa, H.; Drzal, L. *Polymer* **2004**, *45*, 5163.

47. Zhou, Y.; Pervin, F.; Lewis, L.; Jeelani, S. *Mater. Sci. Eng.* **2007**, *452*, 657.

48. Vazquez, A.; Ambrustolo, M.; Moschiar, M. M.; Reboredo, M.; Gérard, J. F. *Compos. Sci. Technol.* **1998**, *58*, 549.

49. Rehmana, A.; Abbas, S. M.; Ammad, H. M.; Badshah, A.; Ali, Z.; Anjum, H. *Mater. Lett.* **2013**, *108*, 253.

50. Lau, K.; Lu, M.; Lam, C.; Cheung, H.; Sheng, F.; Li, H. *Compos. Sci. Technol.* **2005**, *65*, 719.

51. Lavorgna, M.; Romeo, V.; Martone, A.; Zarrelli, M.; Giordano, M.; Buonocore, G. G.; Qu, M. Z.; Fei, G. X.; Xia H. S. *Eur. Polym. J.* **2013**, *49*, 428.

52. Abdalla, M.; Dean, D.; Adibempe, D.; Nyairo, E.; Robinson, P.; Thompson, G. *Polymer* **2007**, *48*, 5662.

53. Pascault, J. P.; Sautereau, H.; Verdu, J.; Williams, R. Thermosetting Polymers; CRC Press, Boca Raton, Florida, United States of America, **2002**; Chapter *2*, p 1.

54. Montazeri, A. *Mater. Des.* **2013**, *45*, 510.

55. Guadagno, L.; De Vivo, B.; Di Bartolomeo, A.; Lamberti, P.; Sorrentino, A.; Tucci, V.; Vertuccio, L.; Vittoria, V. *Carbon* **2011**, *49*, 1919.

56. Coleman, J.; Khan, U; Blau, Gunko, Y. *Carbon* **2006**, *44*, 1624.

57. Kilwon, C.; Lee, D.; Park, C. E.; Huh, W. *Polymer* **1996**, *37*, 813.

58. Tao, K.; Yang, S.; Grunlan, J. C.; Kim, Y.-S.; Dang, B.; Deng, Y.; Thomas, R. L.; Wilson, B. L.; Wei, X. *J. Appl. Polym. Sci.* **2006**, *102*, 5248.

59. Rahman, M.; Hosur, M.; Ludwick, A.; Zainuddin, S.; Kumar, A.; Trovillion, J.; Jeelani, S. *Polym. Test.* **2012**, *31*, 777.

60. Montazeri, A.; Khavandi, A.; Javadpour, J.; Tcharkhtchi, A. *Mater. Des.* **2010**, *31*, 3383.